eLIFE elifesciences.org

RESEARCH ARTICLE

Figures and figure supplements

Frazzled promotes growth cone attachment at the source of a Netrin gradient in the *Drosophila* visual system

Orkun Akin and S Lawrence Zipursky

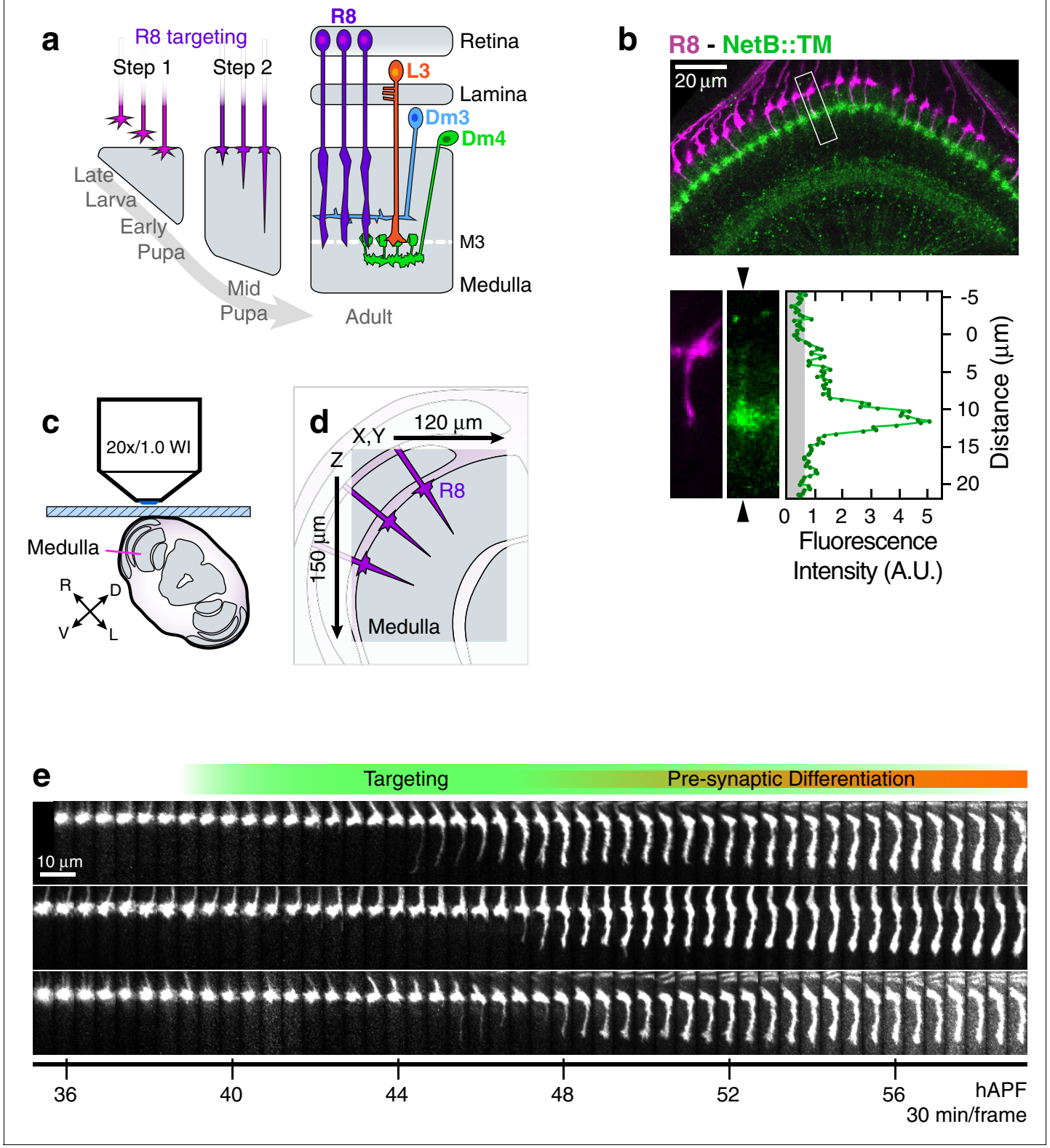

Figure 1. Live imaging of R8 growth cones in the developing fly brain. (**a**) Schematic of R8 targeting. (**b**), *Top panel:* Confocal micrograph of the medulla at 45 hAPF in a fly expressing a membrane-tethered variant of NetB (NetB::TM) from the NetB genomic locus. R8s (magenta, myr::tdTOM) and NetB (green, myc) are shown. *Bottom panels:* Higher magnification view of the boxed region in the top panel; the R8 and NetB::TM channels are

Figure 1 continued on next page

Figure 1 continued

displayed separately. Arrowheads bracketing the NetB::TM image mark the position of the linescan plotted to the right. *Graph:* Linescan of the fluorescence intensity in NetB::TM channel. Gray region marks background values. (**c**) Sample setup. Brain is shown in coronal section, viewed head-on. Body axes, (D)orsal-(V)entral and (R)ight-(L)eft, are marked. (**d**) Detail from (b) illustrates the imaged volume. (**e**) Three growth cones from the same WT brain. Panels were individually contrast enhanced to reveal dimmer features. See ***Figure 1—figure supplement 1*** for a description of the image processing work-flow.

DOI: 10.7554/eLife.20762.003

The following source data is available for figure 1:

Source data 1. Contains numerical data plotted in ***Figure 1b***.

DOI: 10.7554/eLife.20762.004

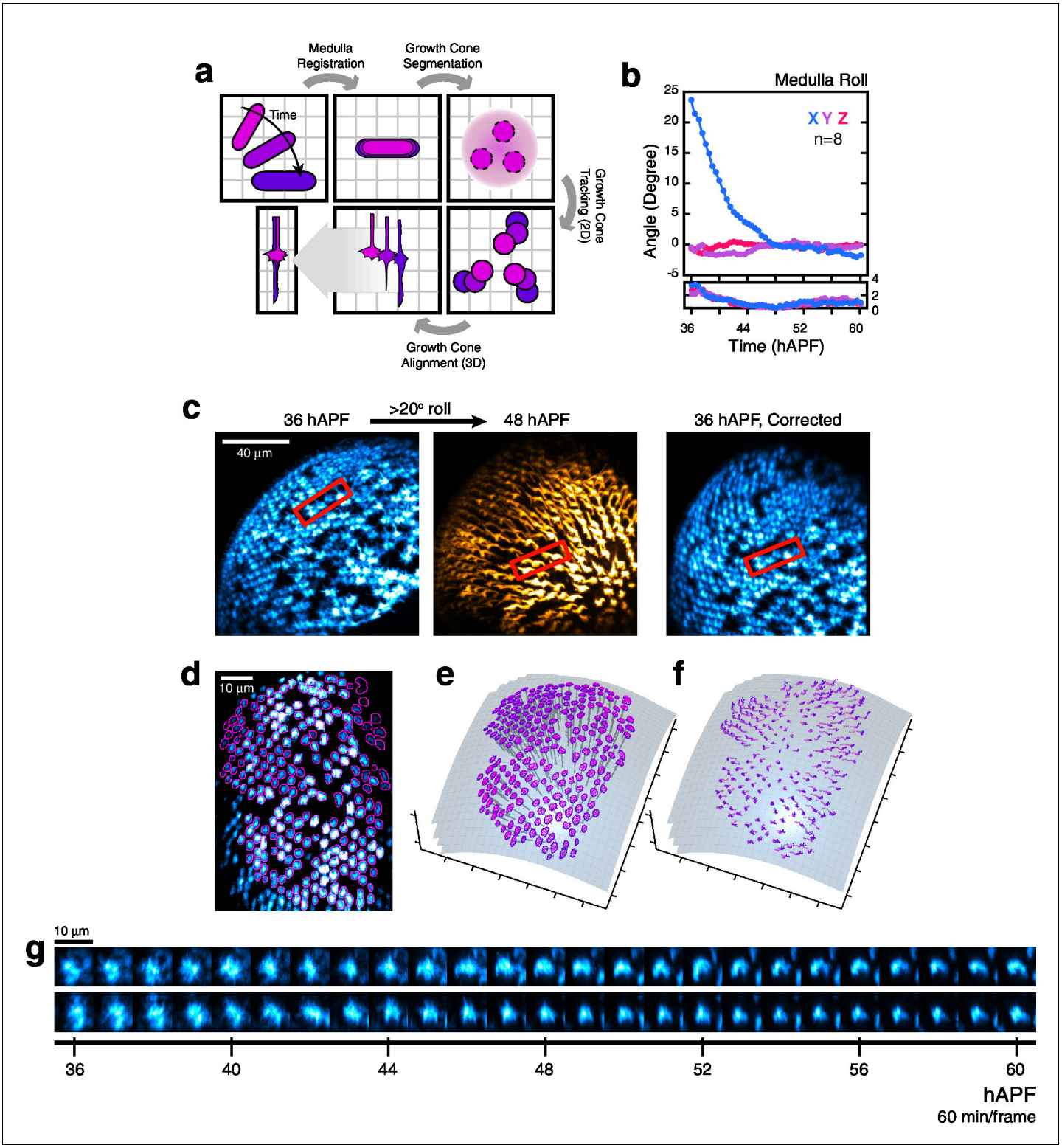

Figure 1—figure supplement 1. Processing 2-photon time series. (**a**) Major steps of the image processing work-flow: Medulla Registration: The R8 array is treated as a rigid body to correct for developmental movement. Segmentation: One stack is used to perform the only segmentation step of the work-flow. Medulla column orientations are also determined at this step. Tracking: Growth cones are tracked through the time series. Alignment: Growth cones are aligned to themselves in 3D over the time series. (**b**) The principal movement during imaging is the roll of the medulla about the horizontal axis of the imaging plane (i.e. X), corresponding to the ventral-right to dorsal-left body axis. Mean (top) and standard deviation (bottom) of the 3-axis rotations are plotted. (**c**) Left: Medulla roll over 12 hr. Images are displayed with cyan-hot and yellow-hot look-up-tables (LUTs) to capture

Figure 1—figure supplement 1 continued on next page

Figure 1—figure supplement 1 continued

more of the dynamic range with limited saturation. Red rectangles mark the same group of growth cones. Gaps in the R8 array are due to a stochastic element in our labeling system. Right: The 36 hr image, after medulla registration. (**d**) Segmented growth cones are outlined in magenta in a maximum intensity projection of the medulla. Image is displayed with a cyan-hot LUT. (**e**) Outlined growth cones in (d) plotted on the outer medulla surface. Medulla column vectors are shown as descending gray lines. (**f**) Growth cone tracks on the outer medulla surface plot their movement. Deeper shades of magenta denotes time progression. (**g**) Tracking output for two growth cones from (d). Images are displayed with a cyan-hot LUT. Data are shown at 1/6 th of the full time resolution (10 min/frame).

DOI: 10.7554/eLife.20762.005

The following source data is available for figure 1:

Figure supplement 1—Source data 1. Contains numerical data plotted in ***Figure 1—figure supplement 1b***.

DOI: 10.7554/eLife.20762.006

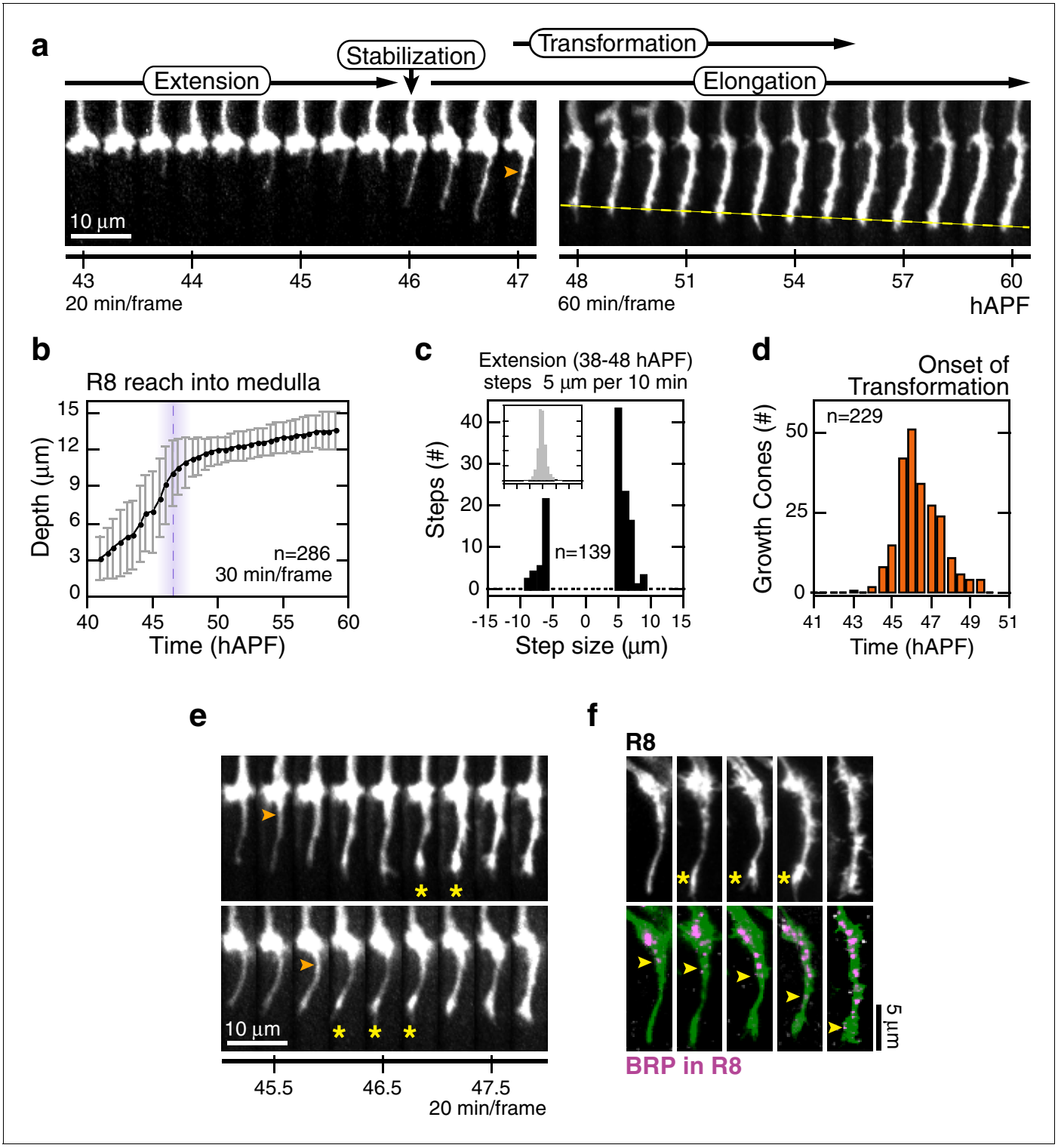

Figure 2. Wild-type R8 targeting. (**a**) Steps of WT targeting. Orange arrowhead marks the onset of *transformation*. Dashed yellow line marks R8 depth through *elongation*. See also ***Figure 3—figure supplement 1b*** for an illustration of transient excursions from the target layer after *stabilization*. (**b**) Average reach of the R8 tip into the medulla (2 animals). Error bars are standard deviation. Dashed magenta line and band mark *stabilization*. (**c**) Counts of frame-to-frame (Δt = 10 min) tip movements equal to or greater than ±5 µm during *extension* (3 animals). Inset is the full distribution of steps, the tails of which are plotted in the parent graph. (**d**) Onset of *transformation* (3 animals). (**e**) *Transformation* proceeds from both ends. Orange arrowheads mark the first frames in which the proximal length of the thin process begins to expand. Yellow asterisks mark the expansion of the tip; see also (f). (**f**) Brp, a marker for presynaptic differentiation, accumulation follows anterograde expansion (yellow arrows) during *transformation*. Panels show

Figure 2 continued on next page

Figure 2 continued

confocal images taken at 47–49 hAPF. R8s are labeled with myr::GFP. R8s express V5-tagged Brp using the STaR system (***Chen et al., 2014***). Overlay of the Brp channel with a mask of the GFP channel highlights R8-localized puncta in magenta.

DOI: 10.7554/eLife.20762.008

The following source data is available for figure 2:

Source data 1. Contains numerical data plotted in ***Figure 2b,c,d***.

DOI: 10.7554/eLife.20762.009

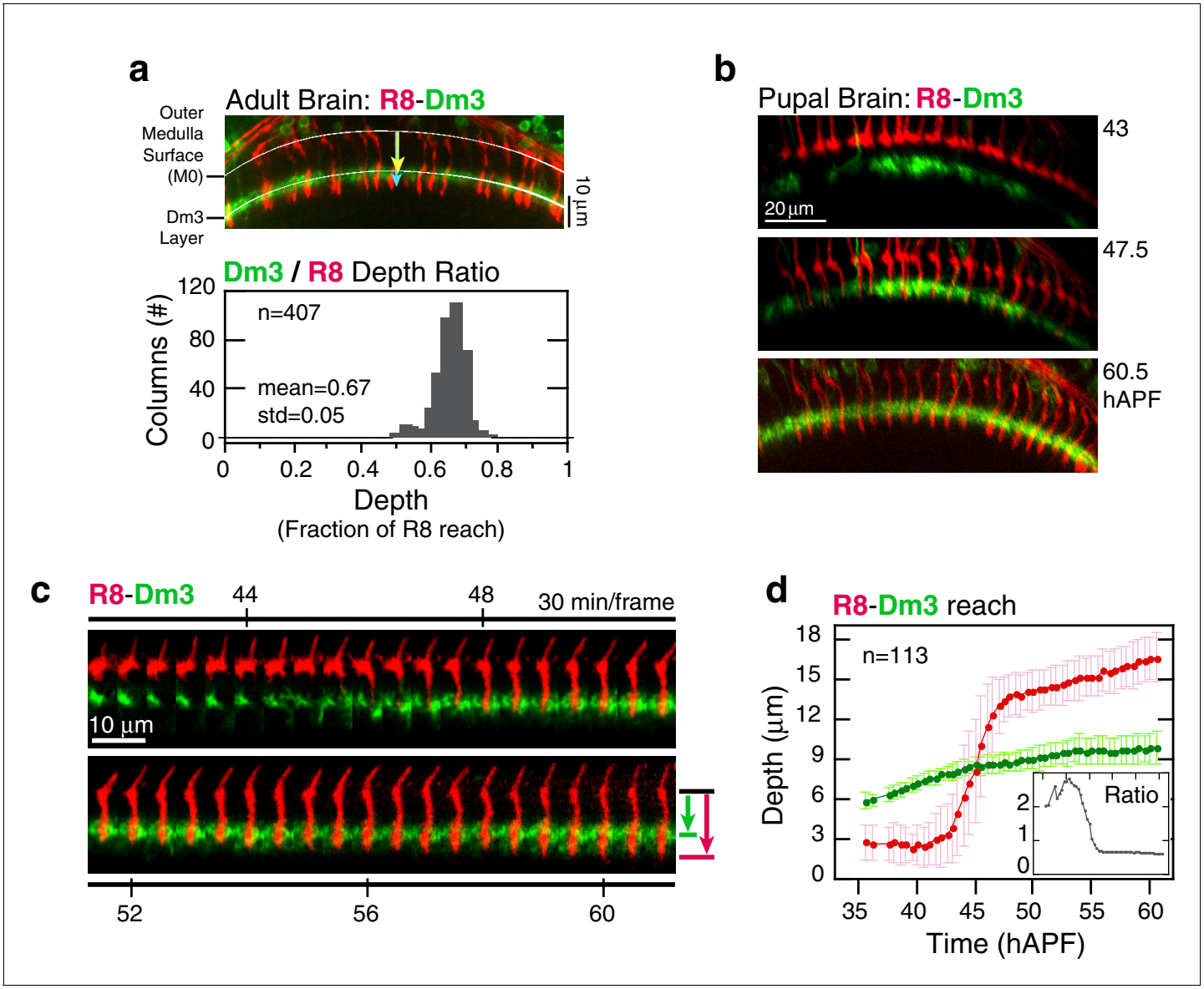

Figure 3. Analysis of *elongation*. (**a**) *Panel:* Confocal micrograph of the outer medulla in the adult brain. R8s (red, myr::tdTOM) and Dm3s (green, myr::GFP) are shown. White arcs are fits to M0 and to the Dm3 processes. Arrows, yellow and blue, mark the distance from M0 to the Dm3 layer and to the R8 tips. *Graph:* Ratio of Dm3 and R8 depths in the brain from panel (n = 407). (**b**) Live imaging of R8 and Dm3. Panels from live imaging of the adult brain in (**a**). The view presented, matching the confocal micrograph in (**a**), was generated post-processing. Panels were individually contrast enhanced to reveal dimmer features. Note that Dm3 processes complete their expansion into layer M2-3 during the window of observation. Despite the incomplete coverage at early time-points, the representation of Dm3 throughout the time-series is sufficient to calculate a surface fit to this fiducial layer marker (see Materials and methods). (**c**) Time series of an R8 and underlying Dm3 process, a fiducial marker for the M2/M3 boundary. Red and green arrows illustrate the measurements plotted in (d). (**d**) Average reach of the R8 tip (red arrow in (c)) and the Dm3 distance from M0 (green arrow in (**c**)), measured in one brain. Error bars are standard deviation. *Inset:* Ratio of the Dm3 distance to M0 and the R8 tip reach. Mean ratio between 50–60 hAPF is 0.65 ± 0.06.

DOI: 10.7554/eLife.20762.011

The following source data is available for figure 3:

Source data 1. Contains numerical data plotted in ***Figure 3a,d***.

DOI: 10.7554/eLife.20762.012

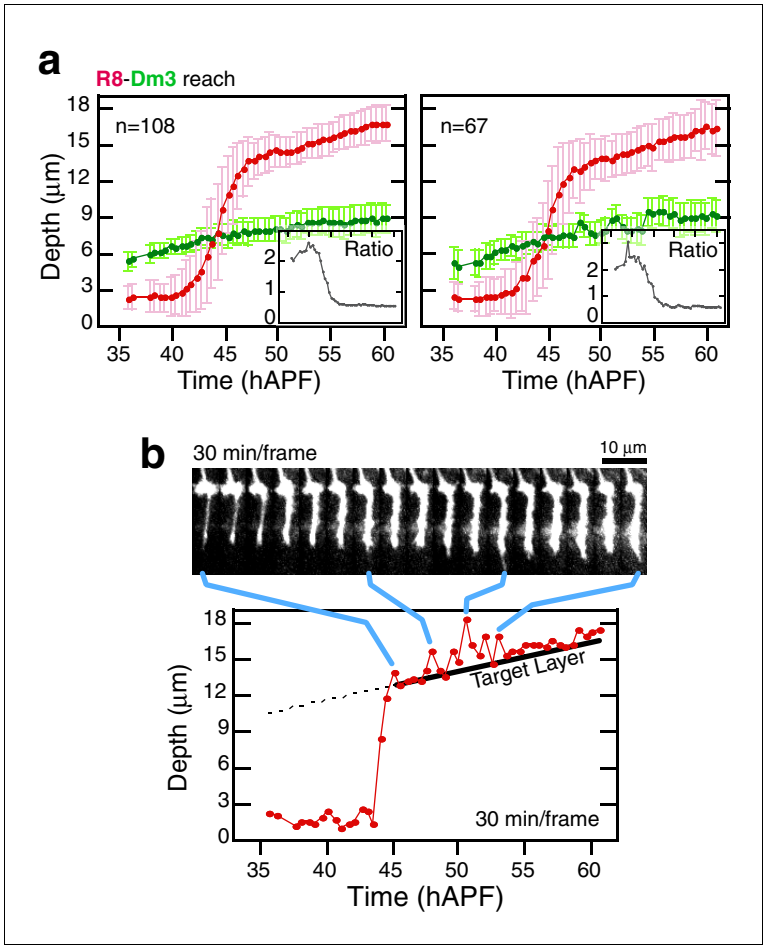

Figure 3—figure supplement 1. Analysis of elongation. (a) Data from two additional brains analyzed as in ***Figure 3d***. (b), Intensity saturated time series highlights transient projections from the target layer during elongation. Tip trace is plotted below; blue connectors map data points to source image panels. The target layer is traced in black.

DOI: 10.7554/eLife.20762.013

The following source data is available for figure 3:

Figure supplement 1—Source data 1. Contains numerical data plotted in ***Figure 3—figure supplement 1a,b***.

DOI: 10.7554/eLife.20762.014

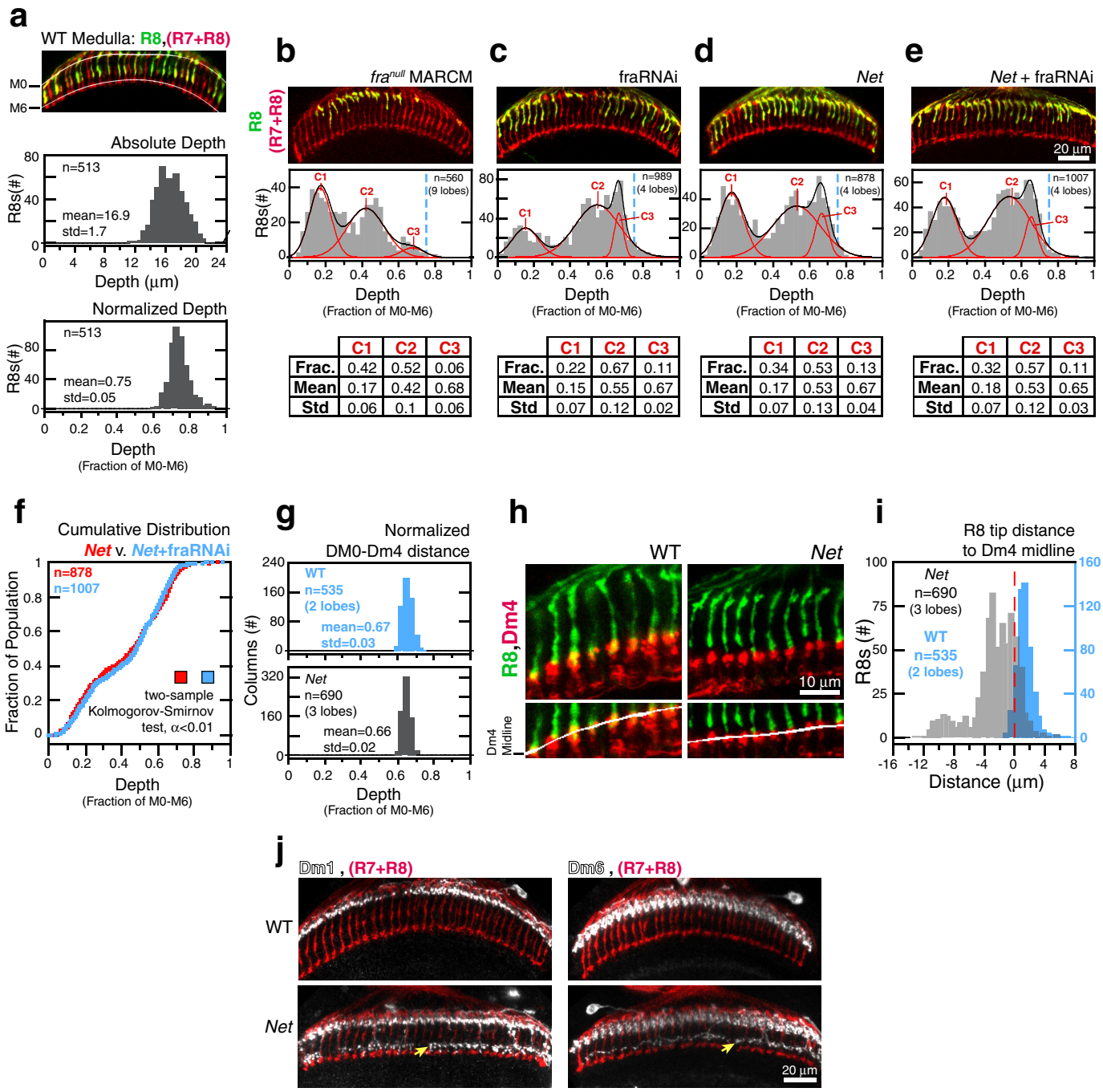

Figure 4. *Fra* and *Net* are in the same genetic pathway for R8 targeting. (**a**) *Panel:* Confocal micrograph of outer medulla. R8s (green, ~70% expressing myr::GFP) and all R cells (red, labeled with Mab24B10) are shown. *Graphs:* Absolute (top) and normalized (bottom) distance between M0 and the R8 tips measured in medulla. (**b**) *Panel:* Confocal micrograph of outer medulla in a MARCM brain. fra^{null} R8s (green, expressing UtrnCH::GFP) and all R cells (red, labeled with Mab24B10) are shown. Projection depths of fra^{null} R8s were measured using a membrane-targeted marker (myr::tdTOM, not shown). *Graph:* Normalized fra^{null} R8s projection depths. Components (C1-3) for the Gaussian Mixture Model (GMM) fit to the distribution are plotted in red; black trace is the sum of the components. Dashed blue line marks the mean of the WT distribution from (**a**). *Table:* GMM parameters. Frac.: fractional contribution of each component to the fit. (**c**) *Panel:* Adult brain in which *fra* expression was knocked down in R8s using a cell-type specific driver (i.e. fraRNAi). Cell labeling as in (a). *Graph:* Normalized projection depths for fraRNAi R8s. *Table:* GMM parameters. (**d**) *Panel: Net* adult brain. Cell labeling as in (a). *Graph:* Normalized R8 projection depths in *Net* animals. *Table:* GMM parameters. (**e**) *Panel: Net* adult brain in

Figure 4 continued on next page

Figure 4 continued

which *fra* expression was knocked down in R8s using a cell-type specific driver (i.e. *fra* RNAi). Cell labeling as in (a). *Graph:* Normalized R8 projection depths in the *Net+fra* RNAi background. *Table:* GMM parameters. (**f**) Cumulative distribution of data in (d) and (e). The distributions are not distinguishable by the two-sample Kolmogorov-Smirnov test at significance level $\alpha < 0.01$. (**g**) Comparison of the normalized distance from M0 to the midline of the Dm4 processes near M3 in WT (top, blue) and *Net* (bottom, gray) male adult brains. (**h**) Confocal micrographs of the outer medulla in WT (left) and *Net* (right) adult brains. R8s (green, myr::GFP) and Dm4s (red, myr::tdTOM) are shown. White curves are fits to the Dm4 midline. (**i**) Absolute distance between R8 tips and the Dm4 midline (dashed red line at 0) measured in WT (blue) and *Net* (gray) adult brains. Positive values indicate that the R8 tip is past the Dm4 midline. (**j**) Two additional cell types with altered morphologies in the *Net* background. Dm1 and Dm6 are both multi-columnar amacrine cells with processes at M1 in the WT (top row). Both cell types generate extra arborizations at M4-M5 (bottom row, yellow arrows) in *Net* animals. Dm1s and Dm6s expressing myr::tdTOM (white) were visualized with immunohistochemistry. Mab24B10 was used to stain for all photoreceptors (red).

DOI: 10.7554/eLife.20762.016

The following source data is available for figure 4:

Source data 1. Contains numerical data plotted ***Figure 4a,b,c,d,e,f,g,i***

DOI: 10.7554/eLife.20762.017

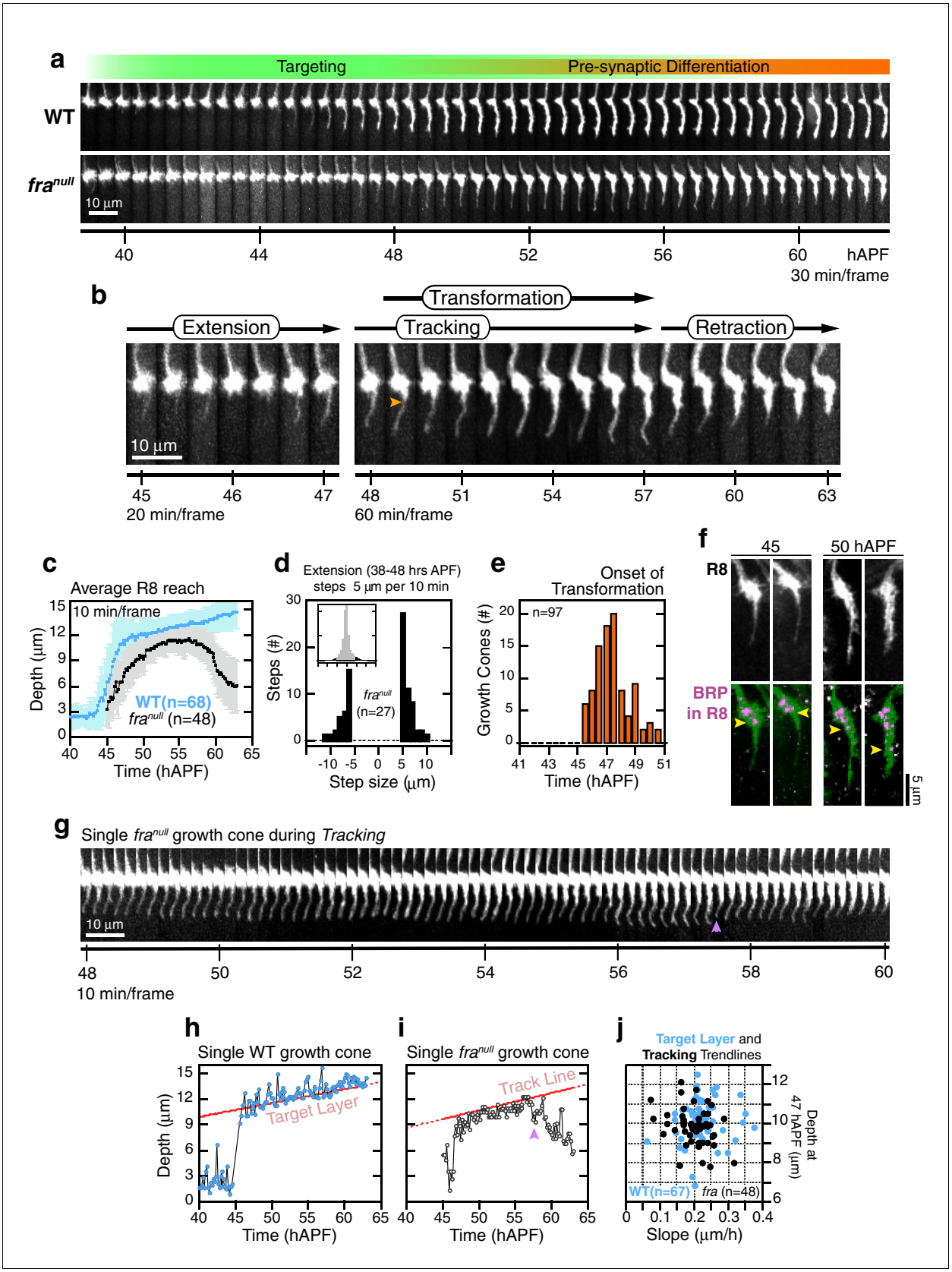

Figure 5. *fra*^{null} R8 targeting. (**a**) Wild-type and *fra*^{null} growth cones from the same mosaic brain. (**b**) Steps of *fra*^{null} targeting. Orange arrowhead marks the onset of *transformation*. (**c**) Data for WT and *fra*^{null} R8s from the same brain presented as in ***Figure 2b***. Note that the apparent difference between

Figure 5 continued on next page

Figure 5 continued

WT and *fra*^{null} reach prior to retraction is due to the opposing effects on this population average metric of (1) transient extensions beyond the target layer in the WT (***Figure 3—figure supplement 1b***) and (2) the retractions of mutant growth cones during *tracking* (see text). For other datasets in which the difference in average reach is less pronounced, see ***Figure 5—figure supplement 1c,d***. (**d**) Data for *fra*^{null} R8s presented as in ***Figure 2c***. (**e**) Data for *fra*^{null} R8s presented as in ***Figure 2d***. (**f**) Brp accumulation follows anterograde expansion (yellow arrows) during *transformation* in *fra*^{null} growth cones. Panels show confocal images of *fra*^{null} R8 growth cones in MARCM brains at 45 and 50 hAPF. R8s are labeled with myr::GFP and myr::tdTOM (MARCM label, not shown). R8s express V5-tagged Brp using the STaR system (*19*). Overlay of the Brp channel with a mask of the GFP channel highlights R8-localized puncta in magenta. (**g**) *fra*^{null} dynamics during *tracking;* growth cone in (b) reproduced at full time resolution. Magenta arrowhead marks a transient retraction. See ***Figure 5—figure supplement 2*** for more examples. (**h**) Tip trace of the WT growth cone in (a), plotted at 10 min resolution. The target layer, in red, is calculated as described in Materials and methods. (**i**) Tip trace of the *fra*^{null} growth cone in (b) and (g), plotted at 10 min resolution. Magenta arrowhead marks the transient retraction shown in (g). The track line, in red, is calculated as described in Materials and methods. (**j**) Scatter plot of slopes and positions of target layer and tracking trendlines at 47 hAPF, for the WT and *fra*^{null} growth cones in (c). The 47 hAPF position is a surrogate for the y-intercept of the trendlines.

DOI: 10.7554/eLife.20762.018

The following source data is available for figure 5:

Source data 1. Contains numerical data plotted ***Figure 5c,d,e,h,i,j***.

DOI: 10.7554/eLife.20762.019

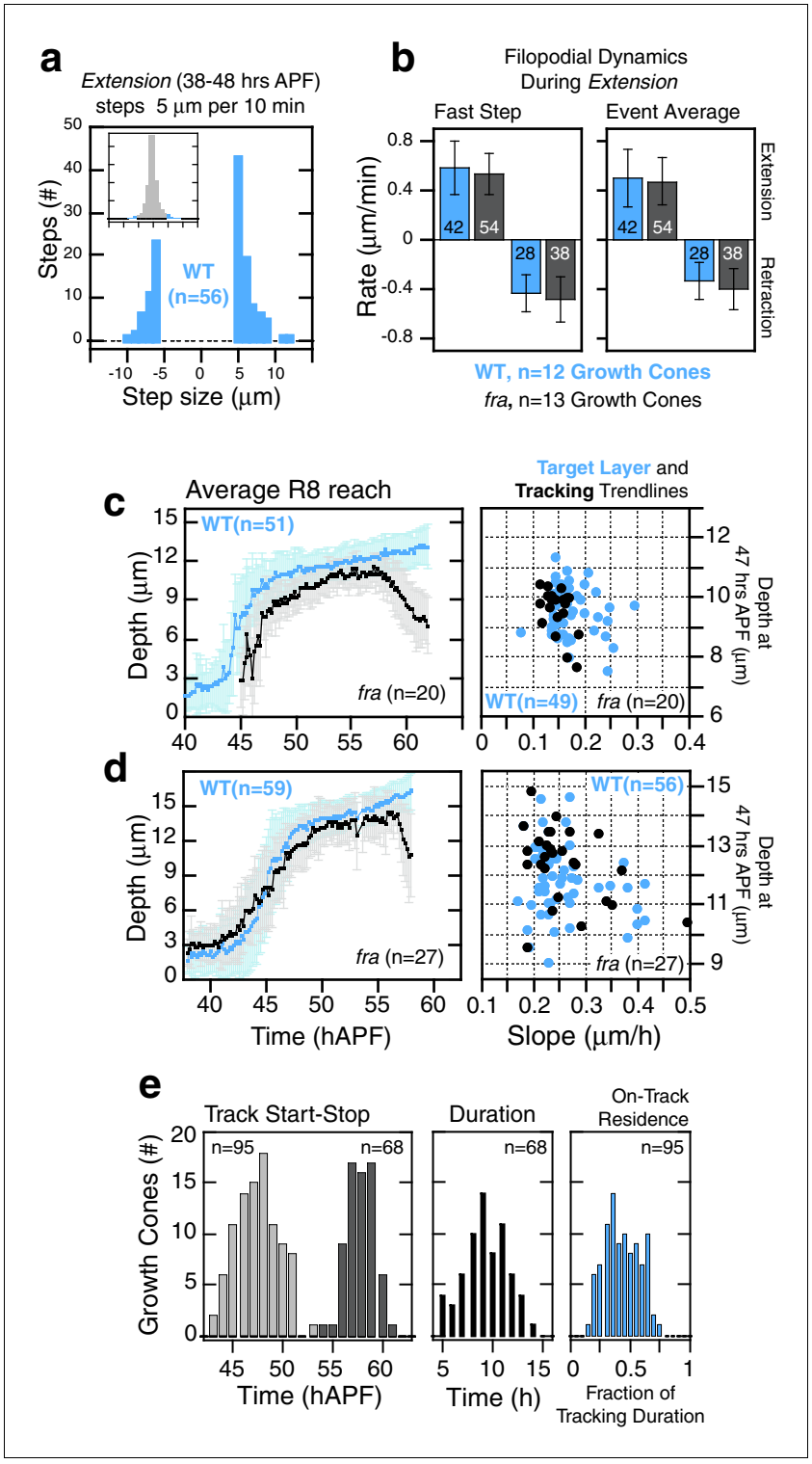

Figure 5—figure supplement 1. *fra*^{null} R8 targeting. (**a**,**b**) Extension dynamics are not altered in *fra*^{null}R8s. (**a**) shows counts of frame-to-frame (Δt = 10 min) tip movements equal to or greater than ±5 µm for WT R8s from the same brain as the *fra*^{null} R8s in ***Figure 5d***. Insets are the full distributions of steps, the tails of which are plotted in the parent graphs. Bar graphs in (**b**) display rate metrics for individual extension and retraction events for wild-type (n = 12) and *fra*^{null} (n = 13) growth cones. 'Fast step' is the largest tip displacement observed between consecutive frames (Δt = 10 min) presented as rate of movement; 'Event average' is the ratio of the total displacement to the total time for a single extension or retraction event. Embedded numbers count the events scored; only extension

Figure 5—figure supplement 1 continued on next page

Figure 5—figure supplement 1 continued

or retraction events with the largest step ≥ 2.5 μm (i.e. ≥ 0.25 μm/min) were considered. Error bars are standard deviation. Wild-type and fra^{null} distributions for any of the 4 metrics presented are not distinguishable by the two-sample Kolmogorov-Smirnov test at significance level $\alpha = 0.05$. (**c**,**d**) Average reach into the medulla (see ***Figure 5c***) and target layer and tracking trendline metrics (see ***Figure 5j***) from two additional MARCM experiments. (**e**) Tracking metrics (3 animals). Track Start and Stop are the times of initial arrival (light gray) at and final retraction (dark gray) from the track line (i.e. target layer), respectively. Tracking duration is calculated for each growth cone. On-Track residence (blue) is the fraction of time each growth cone spends above the track line.

DOI: 10.7554/eLife.20762.020

The following source data is available for figure 5:

Figure supplement 1—Source data 1. Contains numerical data plotted in ***Figure 5—figure supplement 1a,b,c,d,e***.

DOI: 10.7554/eLife.20762.021

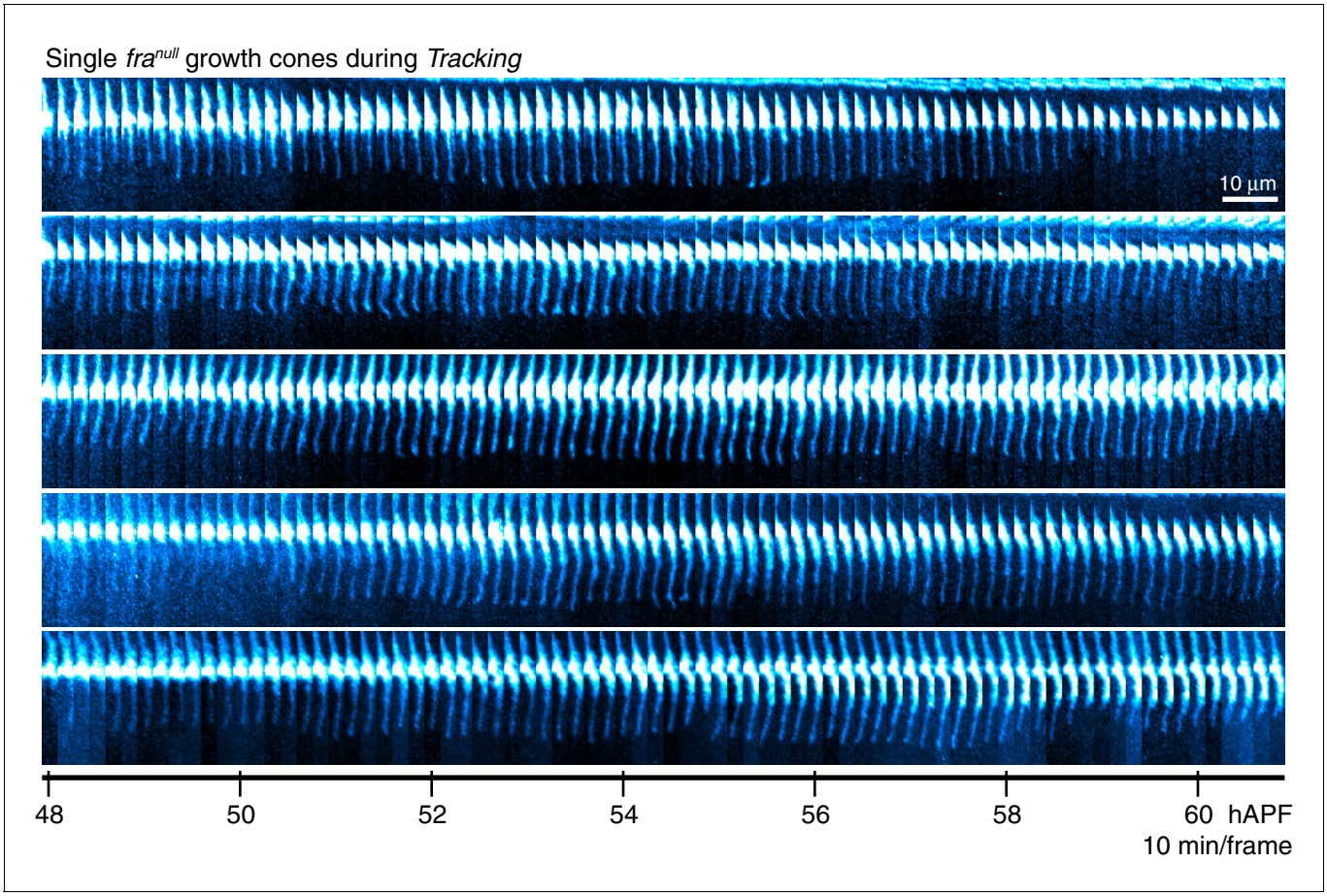

Figure 5—figure supplement 2. *fra*^{null} dynamics during tracking Single *fra*^{null}growth cones presented at full time resolution.Images are shown with a cyan-hot look-up table to increase displayed dynamic range.
DOI: 10.7554/eLife.20762.022

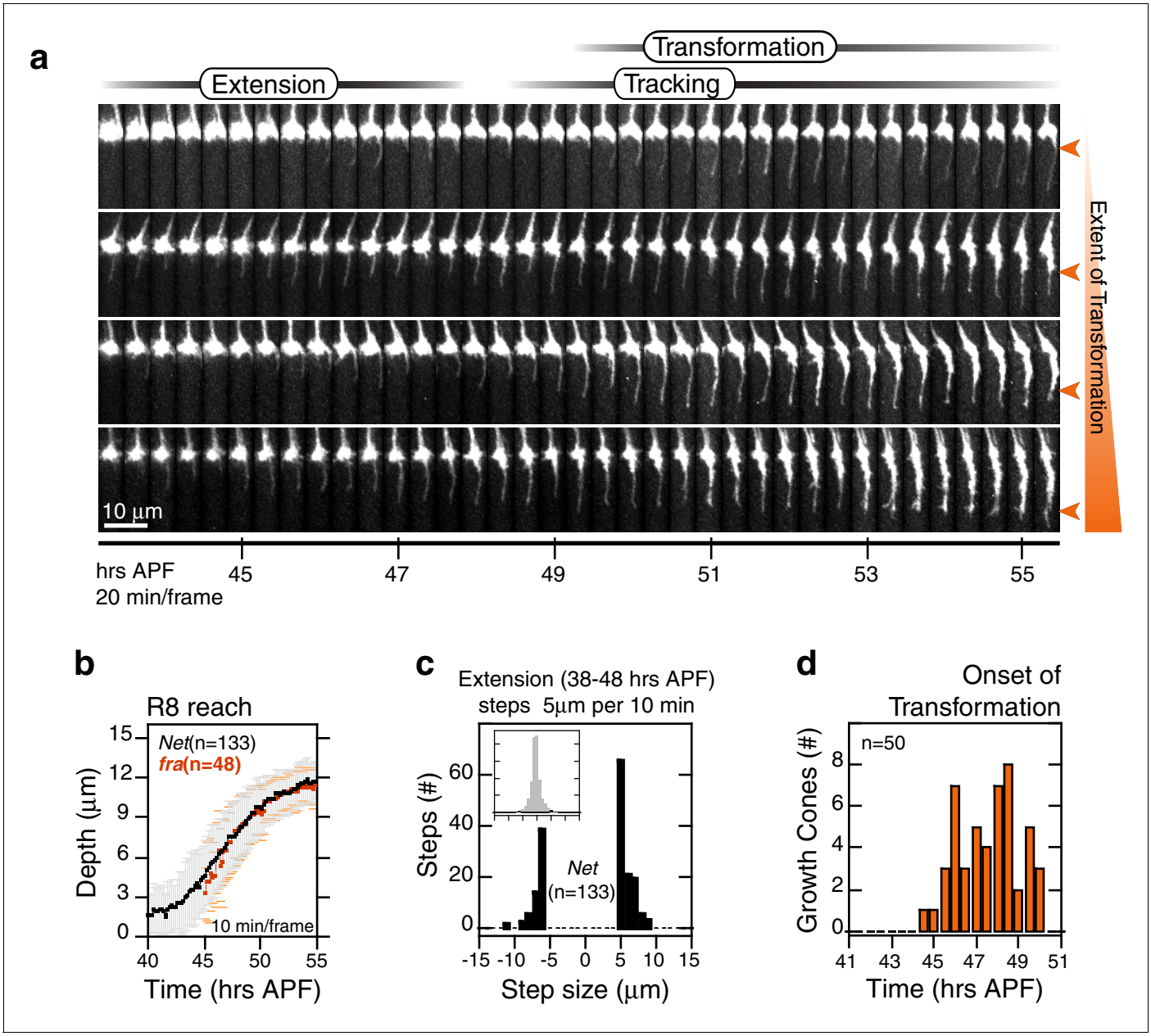

Figure 6. R8 targeting in *Net* mutants. (**a**) Four growth cones from the same *Net* null mutant brain. Orange arrowheads mark the extent of *transformation* at the end of the time series in this data set; this determines the final R8 depth after retraction of the thin process. (**b**) Data for R8s in a *Net* mutant brain presented as in ***Figure 2b***. The corresponding trace for fra^{null} R8s from ***Figure 5c*** is reproduced in orange. (**c**) Data presented as in ***Figure 2c***. (**d**) Data for presented as in ***Figure 2d***.

DOI: 10.7554/eLife.20762.025

The following source data is available for figure 6:

Source data 1. Contains numerical data plotted in ***Figure 6b,c,d***.

DOI: 10.7554/eLife.20762.026

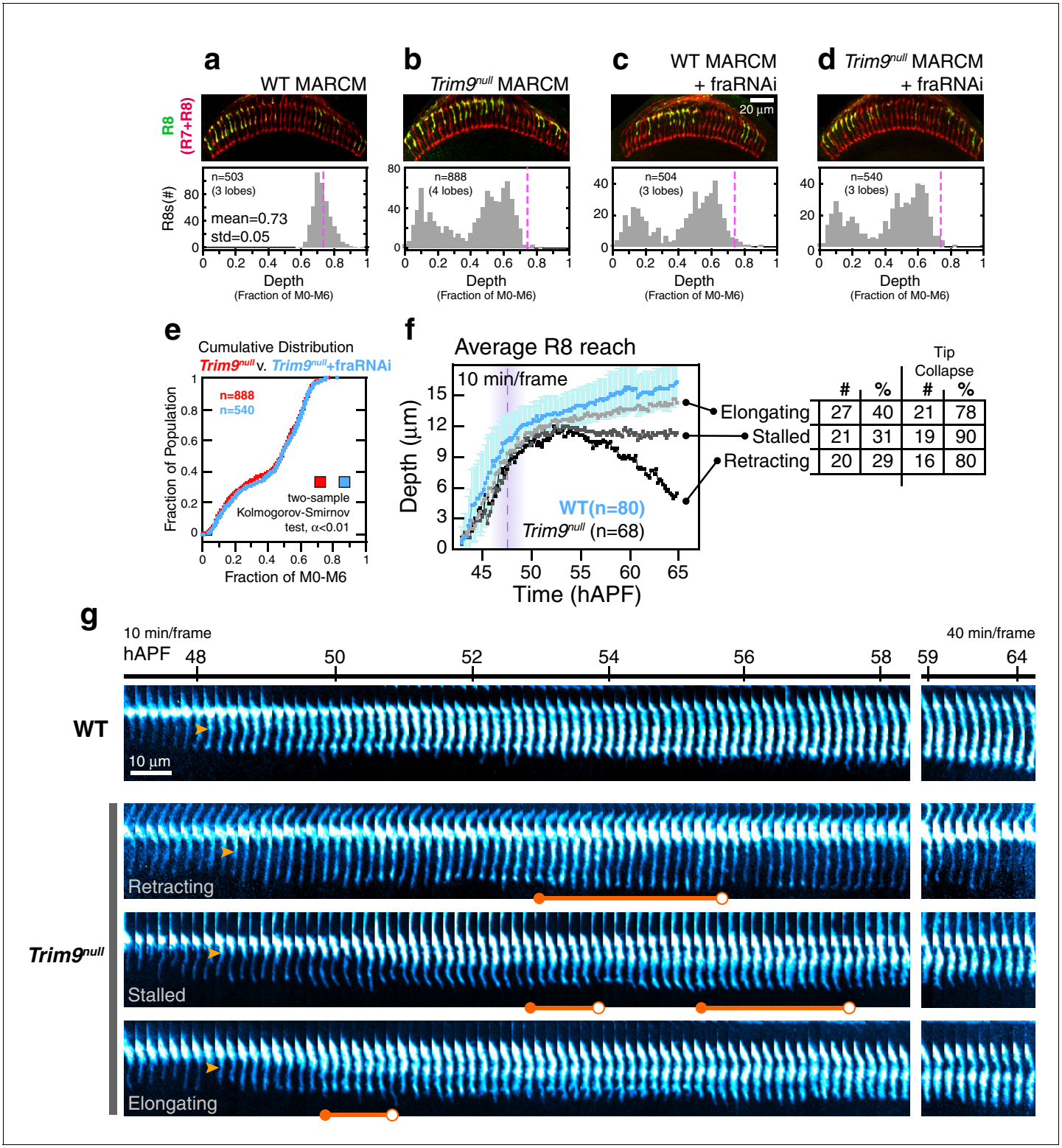

Figure 7. *Trim9*^{null} R8 targeting. (**a**) *Panel:* Confocal micrograph of outer medulla in a WT MARCM brain. MARCM labeled WT R8s (green, expressing UtrnCH::GFP) and all R cells (red, labeled with Mab24B10) are shown. *Graph:* Normalized R8s projection depths. Dashed pink line marks the mean of the distribution. (**b**) *Panel:* Confocal micrograph of outer medulla in a *Trim9*^{null} MARCM brain. Cell labeling as in (**a**). *Graph:* Normalized R8s projection depths. Dashed pink line marks the mean of the WT distribution from (**a**). (**c**) *Panel:* Adult brain in which *Fra* expression was knocked down in R8s using a cell-type specific driver (i.e. fraRNAi) in the WT MARCM setup. *Graph:* Normalized R8s projection depths. Dashed pink line marks the mean of the WT distribution from (a). (**d**) *Panel:* Adult brain in which *Fra* expression was knocked down in R8s using a cell-type specific driver (i.e. fraRNAi) in the

Figure 7 continued on next page

Figure 7 continued

Trim9^{null} MARCM setup. *Graph:* Normalized R8s projection depths. Dashed pink line marks the mean of the WT distribution from (a). (**e**) Cumulative distribution of data in (b) and (d). The distributions are not distinguishable by the two-sample Kolmogorov-Smirnov test at significance level $\alpha < 0.01$. (**f**) Reach of the tip into the medulla for WT and *Trim9*^{null} R8s, compiled from 2 brains. Error bars are standard deviation for WT. Dashed magenta line and band mark *stabilization*. Table shows number and percentage of mutant R8s in each class and for tip collapse events. As virtually all R8 terminals in the adult fall short of the target layer, the *elongating* class of R8 terminals must retract after 65 hr APF. (**g**) Wild-type and *Trim9*^{null} growth cones from the same mosaic brain. Images are shown with a cyan-hot look-up table to increase displayed dynamic range. Orange arrowheads mark the onset of *transformation*. Orange barbells mark prominent expanded tips (closed end) that collapse (open end).

DOI: 10.7554/eLife.20762.027

The following source data is available for figure 7:

Source data 1. Contains numerical data plotted ***Figure 7a,b,c,d,e,f***.

DOI: 10.7554/eLife.20762.028

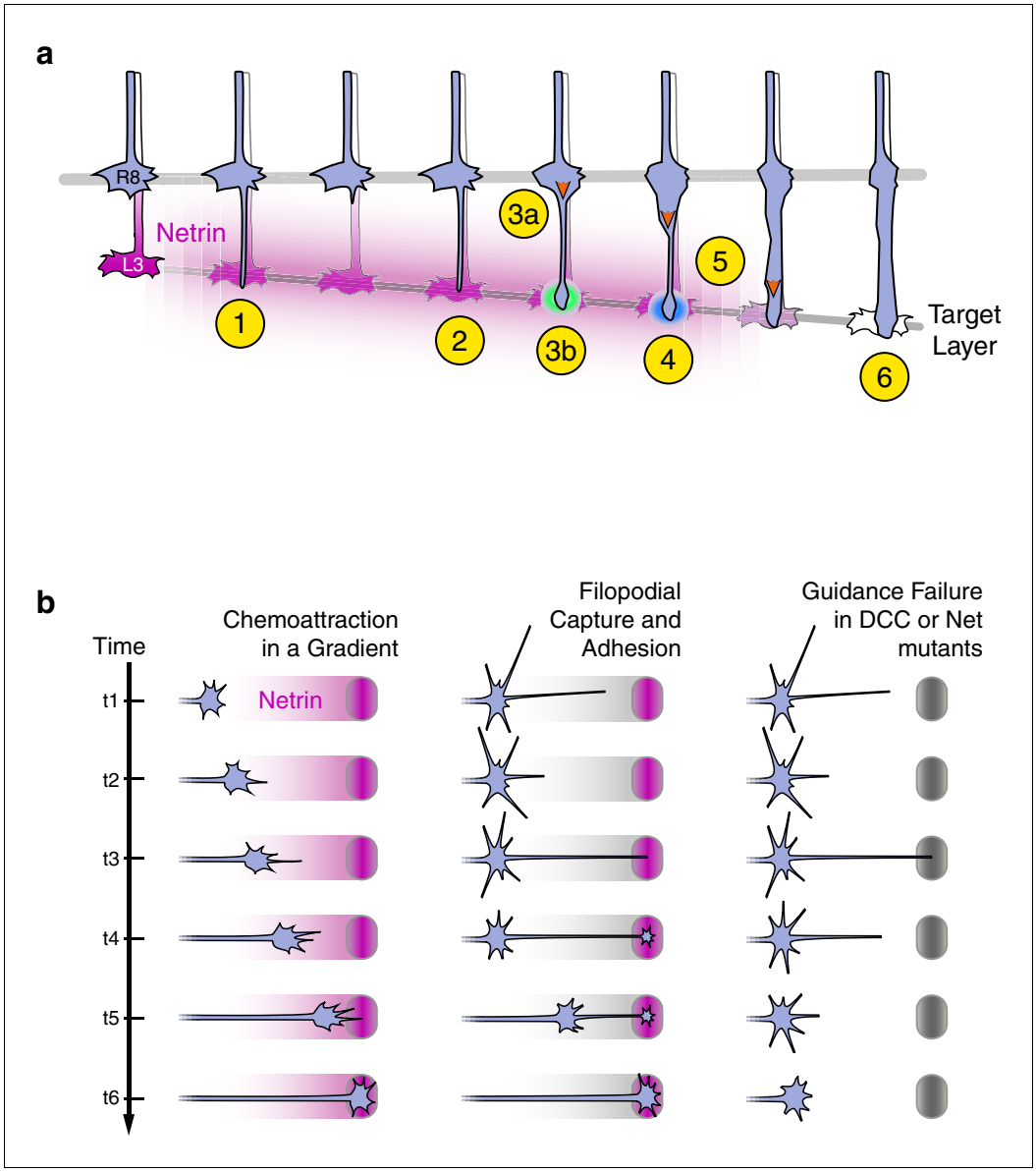

Figure 8. Axon guidance through Net-DCC-mediated adhesion. (**a**) Net-Fra signaling in the second step of R8 targeting: (1) *Extension* of thin process into medulla, Net-Fra independent. (2) Target layer recognition, Net-Fra independent. (3a) Onset of *transformation,* proximal expansion (orange arrowhead), Net-Fra independent. (3b) Tip expansion in the target layer, Net-Fra dependent (cyan highlight). (4) Consolidation of adhesion to the target layer, Net-Fra-Trim9 dependent (blue highlight). (5) Progress of *transformation* (orange arrows). The extent of *transformation* completed before the end of *tracking* in the mutant backgrounds may underlie the difference in expressivity between the *Net*, *fra*^{null}, and *Trim9*^{null} adult phenotypes. (6) *Elongation* and maturation. (**b**) Net-DCC mediated guidance works through target adhesion, not chemoattraction in a gradient. First Column: In the classical view of chemoattraction, DCC-laden filopodia sense the gradient of extracellular Net (pink) and direct the movement of the growth cone toward the source. Second Column: In the alternate model, the Net source is detected independent of the gradient (gray), through filopodial search and capture (t1-t3) or directed extension of a targeting filopodia guided by a separate mechanism (not depicted). Net-DCC signaling at the ligand peak promotes attachment to the target (t4); the growth cone proper then reaches the target with the aid of this initial anchor (t5-t6). Third Column: The generalized view of axon guidance failure in DCC-Net mutants shows that reaching the target does not require the receptor or the ligand; the final phenotype is due to retraction instead of a loss of attraction.

DOI: 10.7554/eLife.20762.029